Optical Materials xxx (2010) xxx–xxx

Contents lists available at ScienceDirect

Optical Materials

journal homepage: www.elsevier.com/locate/optmat

Transparent ceramics for high-energy laser systems

Jas Sanghera [a,*], Shyam Bayya [a], Guillermo Villalobos [a], Woohong Kim [a], Jesse Frantz [a], Brandon Shaw [a], Bryan Sadowski [b], R. Miklos [b], Colin Baker [a], Michael Hunt [c], Ishwar Aggarwal [a], Fred Kung [b], David Reicher [d], Stan Peplinski [d], Al Ogloza [e], Peter Langston [e], Chuck Lamar [f], Peter Varmette [g], Mark Dubinskiy [h], Lewis DeSandre [i]

[a] US Naval Research Laboratory, Washington, DC 20375, United States
[b] GTEC Inc., Crofton, MD 21114, United States
[c] University Research Foundation, Greenbelt, MD 20770, United States
[d] US Air Force Research Laboratory, Kirtland AFB, NM 87117, United States
[e] NAWC, China Lake, CA 93555, United States
[f] US Army Space & Missile Defense Command, Huntsville, AL 35807, United States
[g] SAIC, Huntsville, AL 35806, United States
[h] US Army Research Laboratory, Adelphi, MD, United States
[i] ONR Global, London, UK

ARTICLE INFO

Article history:
Received 5 October 2010
Accepted 21 October 2010
Available online xxxx

Keywords:
Spinel
Transparent ceramics
Laser ceramics

ABSTRACT

We demonstrate that transparent magnesium aluminate spinel ceramic possesses excellent thermo-optical properties, a record low absorption loss of 6 ppm/cm, and superior ruggedness which position it as a prime candidate for an exit window aperture for high energy laser systems, especially in hostile environments. We also demonstrate lasing with an efficiency of about 45% in transparent Yb^{3+}:Y_2O_3 ceramic made by hot pressing high purity submicron co-precipitated powder. This paves the way forward for high power solid state lasers exploiting hosts with higher thermal conductivity than YAG.

Published by Elsevier B.V.

1. Introduction

High-energy laser (HEL) systems have unique material requirements for both the lasing medium and the exit aperture window. The role of the exit aperture is to isolate the lasing medium from the environment and provide protection, without compromising the light propagating through the window. When a high-energy beam transmits through a window material, a part of the laser energy is absorbed by the material and causes optical aberrations. This absorbed energy results in material heating in the local exposed region changing its refractive index based on the materials thermo-optic coefficient (dn/dT), thermal expansion coefficient and stress optic coefficient. These changes result in beam distortion and loss of output power, measured as optical path distortion (OPD), which has a severe impact on system performance. Ideally, the window should possess low absorption loss and be environmentally rugged and strong. The latter enables thinner windows, thereby lowering the weight and further reducing the absorption loss and OPD. Until now, this role has been limited to glasses. For HEL systems operating in the SWIR (1–2 μm) wavelength region, the materials of choice are limited to just a few, including examples such as fused silica and oxyfluoride (OFG) glasses [1]. Some of the HEL systems are expected to operate in harsh environmental conditions where fused silica and OFG glasses will not survive, and so rugged windows are required. We have developed transparent magnesium aluminate spinel ($MgAl_2O_4$) ceramic as a rugged window and dome material for protecting EO/IR sensors operating from the UV to the mid-IR [2]. This paper summarizes the results of our development efforts for spinel as a window for HEL systems.

There are three main high energy lasers systems, namely: gas lasers, free-electron lasers and solid state lasers. The first two possess a very large footprint making mobility a key issue. On the other hand, solid state lasers have significantly smaller footprints and have potential for enhanced mobility. Examples of these include slab, rod and disk type of lasers based on rare earth doped crystals. An example is the Nd^{3+}:YAG (yttrium aluminum garnet) laser which is based on a single crystal of YAG doped with Nd^{3+} ions. More recently, ceramic Nd^{3+}:YAG has been fabricated and used to demonstrate 67 kW [3] and >100 kW [4,5] of output power at 1.06 μm, respectively. This remarkable result has been attributed to the high optical quality ceramic made by vacuum sintering of high purity powder by Konoshima Chemical Company in Japan [6]. Sintering enables fabrication of ceramics at approximately

* Corresponding author.
E-mail address: jasbinder.sanghera@nrl.navy.mil (J. Sanghera).

0925-3467/$ - see front matter Published by Elsevier B.V.
doi:10.1016/j.optmat.2010.10.038

Report Documentation Page

Form Approved
OMB No. 0704-0188

1. REPORT DATE	2. REPORT TYPE	3. DATES COVERED
OCT 2010		**00-00-2010 to 00-00-2010**

4. TITLE AND SUBTITLE	5a. CONTRACT NUMBER
Transparent ceramics for high-energy laser systems	5b. GRANT NUMBER
	5c. PROGRAM ELEMENT NUMBER
6. AUTHOR(S)	5d. PROJECT NUMBER
	5e. TASK NUMBER
	5f. WORK UNIT NUMBER
7. PERFORMING ORGANIZATION NAME(S) AND ADDRESS(ES) **Naval Research Laboratory,Washington,DC,20375**	8. PERFORMING ORGANIZATION REPORT NUMBER
9. SPONSORING/MONITORING AGENCY NAME(S) AND ADDRESS(ES)	10. SPONSOR/MONITOR'S ACRONYM(S)
	11. SPONSOR/MONITOR'S REPORT NUMBER(S)

12. DISTRIBUTION/AVAILABILITY STATEMENT
Approved for public release; distribution unlimited

13. SUPPLEMENTARY NOTES

14. ABSTRACT

We demonstrate that transparent magnesium aluminate spinel ceramic possesses excellent thermo-optical properties, a record low absorption loss of 6 ppm/cm, and superior ruggedness which position it as a prime candidate for an exit window aperture for high energy laser systems, especially in hostile environments. We also demonstrate lasing with an efficiency of about 45% in transparent Yb3+:Y2O3 ceramic made by hot pressing high purity submicron co-precipitated powder. This paves the way forward for high power solid state lasers exploiting hosts with higher thermal conductivity than YAG.

15. SUBJECT TERMS

16. SECURITY CLASSIFICATION OF:			17. LIMITATION OF ABSTRACT	18. NUMBER OF PAGES	19a. NAME OF RESPONSIBLE PERSON
a. REPORT	b. ABSTRACT	c. THIS PAGE			
unclassified	**unclassified**	**unclassified**	**Same as Report (SAR)**	**8**	

two-thirds of the melting temperature and avoids high temperature melting issues such as crucible contamination, chemical inhomogeneity due to volatilization, cracking due to thermal gradients, and inhomogeneities in the rare earth ion dopant concentration. In addition, this process is amenable to fabrication of high optical quality ceramics with controlled and graded dopant concentrations as well as undoped claddings for better thermal management [7]. The low temperature aspect of this process allows one to make ceramics from potentially better laser host materials than YAG which might be difficult to grow as single crystals. One example is Yb^{3+} doped Y_2O_3 which has excellent potential as a laser material for high power lasers operating at 1 μm [8]. Yb^{3+} can be easily pumped with commercial high power diode lasers near 940 nm or 976 nm and has a low quantum defect for laser emission near 1080 nm. This low quantum defect coupled with the high thermal conductivity of Y_2O_3 will result in decreased thermal loading during high laser power operation. However, making large crystals using traditional crystal growing is a problem. This is associated with the high melting point of Y_2O_3 (>2400 °C) leading to crucible interactions and impurity contamination, while the high temperature phase transition at ~2200 °C leads to strain and cracking. These problems can be overcome by making a polycrystalline ceramic using the low temperature ceramization process. We report lasing in transparent Yb^{3+} doped Y_2O_3 ceramic made by hot pressing.

2. Experimental

2.1. Spinel ceramic

Transparent spinel ceramic was made from high purity powder synthesized using aqueous chemical methods. The 5 × 9's pure Al and Mg chloride were mixed together to form a homogeneous solution at 80 °C. Ammonium hydroxide was added dropwise to the solution to form a precipitate that was subsequently filtered, washed with water and then acetone, and baked to dry. The powder was then calcined at 600 °C to convert to magnesium aluminate spinel.

Ceramic spinel was made by hot pressing ball milled spinel powders at 1400–1650 °C for 2–4 h using a uniform coating of a small amount of LiF sintering aid that was eliminated by evaporation prior to full densification. The hot-pressed samples were transparent, with densities greater than 99% of theoretical. The samples were subsequently hot isostatically pressed (HIP) at 1600 °C for 2 h under an Ar gas pressure of 30,000 psi to produce fully dense and transparent ceramics. The samples ranged in size from 5 cm in diameter and 6 mm thick, to larger samples (15 cm diameter) from which smaller samples were cut, ground and polished for many of the measurements. High damage threshold anti-reflective (AR) coatings (SiO_2/ZrO_2) were applied to the surface of polished 5 cm diameter samples using dc-magnetron sputtering [9]. The versatility of the ceramization process was demonstrated by making a large 10 in. diameter transparent spinel ceramic sample which was also coated with low loss broadband AR coatings.

2.2. Yb^{3+} doped Y_2O_3 ceramic

The commercial Yb^{3+} doped Y_2O_3 powder contains many chemical impurities, whose concentration varies from lot-to-lot and also within a given lot. This leads to poor sintering and causes high absorption and scattering losses. Therefore, we prepared high purity Yb^{3+}:Y_2O_3 powder by co-precipitation using an aqueous process. In this case, the individual nitrates (5 × 9's purity) were dissolved in de-ionized water to form a mixed nitrate solution containing Y^{3+} and Yb^{3+} ions. Ammonium hydroxide solution was added to the nitrate solution to co-precipitate the mixed hydroxides which were subsequently filtered, washed with water and then acetone, dried and finally calcined at 600 °C to convert to Yb^{3+}:Y_2O_3 powder. Most of the results reported in this paper refer to a concentration of 2 mol% Yb^{3+} relative to Y^{3+}, although we did make powder and ceramics with different concentrations of Yb^{3+}.

Ceramic Yb^{3+}:Y_2O_3 was made by hot pressing ball milled powders at 1550 °C for 2 h, also using a uniform coating of a small amount of LiF sintering aid that was eliminated by evaporation prior to full densification. The hot pressed powder was partially transparent with a density of approximately 99% and was subsequently hot isostatically pressed (HIP) to produce transparent Yb^{3+}:Y_2O_3 ceramic. The hot pressing and HIP procedures were performed well below the melting point of 2400 °C and the phase transition temperature of ~2200 °C associated with Y_2O_3.

2.3. Characterization

The crystal phase, morphology and purity of the powders and ceramics were characterized using X-ray diffraction, scanning electron microscopy, and glow discharge mass spectroscopy. Additionally, the powder surface area was measured using microporismetry (BET method).

Transmission measurements on polished ceramics were performed using UV–vis and FTIR spectrometers and refractive indices were measured using ellipsometry (J. Woollam and Co.). The absorption loss of the bulk spinel and the AR coatings was measured using the photo-thermal common path interferometric technique [10].

The thermo-optic coefficient (dn/dT) and stress optic coefficient were measured using Fizeau interferometer [11,12] at 1.3 μm and optical retardation under uniaxial load [13], respectively. Densities were measured using the Archimedes method, Vickers hardness was measured using a diamond tip micro indentor at a 200 g load, and Young's modulus and Poisson ratio were measured using impulse excitation of vibration method [14]. The fracture strength was measured using polished rods with dimensions of 3 × 4 × 45 mm using a standard four point bend test at University of Dayton Research Institute, OH. Thermal expansion coefficient of 1 in. long rods was measured using a dilatometer from room temperature to 200 °C. The heat capacity was measured using a differential scanning calorimeter [15], and the thermal conductivity was calculated from the measured thermal diffusivity [16].

Rain and sand erosion tests were performed on polished spinel samples. The rain erosion tests were conducted at 600 mph for a duration of 20 min using 2 mm rain droplets, flowing at 6–7 droplets/s, and impinging on the surface of the samples at 90°. The sand erosion tests were performed at 460 mph for 20 min using sand particle sizes in the range of 88–105 μm, with a mass/load ratio of 0.02 g/cm^2, and impinging the sample surface at 90°.

AR coated samples were characterized using visible-IR spectroscopy, MIL-C-675C Adhesion Test and MIL-C-48497 Severe Abrasion Test. White light interferometry and atomic force microscopy (AFM) were used to characterize the surface roughness of polished samples and the AR coated surfaces.

The fluorescence lifetime of the Yb^{3+}:Y_2O_3 powder and ceramic was measured by pumping at 940 nm using a low power diode laser.

2.4. Laser oscillation

Small 3 mm diameter samples of 2% Yb^{3+}:Y_2O_3 ceramic were obtained by core drilling the large samples. Both surfaces were polished to a high optical quality (<2 nm rms surface roughness). One surface was coated for high reflectivity (>99.9%) at 1076 nm in

order to form the input coupler of the laser cavity mirror. This surface was also coated for high transmittance at 940 nm, the pump wavelength. An anti-reflective coating for 1076 nm was applied to the sample's other surface. The sample was wrapped along its circumference with a thin piece of indium foil and inserted into a copper heat sink that was cooled with chilled water to a temperature of 15 °C.

A fiber-coupled 940 nm diode laser (LIMO GmbH) with a maximum output power of 20 W was used as a pump. The pump beam was collimated and then focused to a spot with a diameter of approximately 280 μm. A dielectric mirror with a radius of curvature of 25 cm was placed approximately 1 cm from the output surface of the sample to act as the laser's output coupler. Several mirrors, with reflectivities ranging from 90% to 99% at 1076 nm were tested in order to find the optimum output coupling.

In order to characterize the Yb^{3+}:Y_2O_3 laser in CW mode, constant current was applied to drive the pump diode. A square wave with a frequency of 127 Hz and a 50% duty cycle was used to drive the pump diode to characterize the laser in quasi-CW mode. The absorbed pump power, measured by placing a power meter beyond the pump's focus, was assumed to be the difference between the powers with and without the Yb^{3+}:Y_2O_3 sample and the appropriate filters in place. The output power was measured by placing a calibrated pyroelectric detector, with appropriate filters attached, beyond the output coupler. The spectral characteristics of the laser were measured with an optical spectrum analyzer.

Pulsed lasing experiments were also performed on the same ceramic sample. The sample was placed in a 27.5 cm long laser cavity using an output coupler reflectivity of 95% with a radius of curvature 30 cm. The pump laser operated at 936 nm with a repitition rate of 10 Hz and pulse width of 1 ms.

3. Results and discussion

3.1. Spinel ceramic

Spinel powder synthesized by the aqueous process produced approximately 100–200 nm crystallites (Fig. 1) with excellent phase purity as highlighted by X-ray diffraction analysis (Fig. 2) and chemical analysis (Table 1). Compared to commercial powder, the impurity content is several orders of magnitude lower. The surface area of the synthesized powder was 25 m^2/g compared with a range of 10–30 m^2/g for commercial powder.

The ceramics made from our powder exhibit excellent visible and infrared transparency. Fig. 3 shows an uncoated 5 cm diameter window and a 10 in. diameter window coated with broadband AR coatings. Fig. 4 shows the transmission spectrum compared with silica glass and sapphire, and highlights the superior infrared transmission of spinel. The grain size ranges from about 100 μm to 25 μm for samples densified at 1650 °C to 1500 °C, respectively. While the transmission was unaffected by grain size since the grain boundaries are relatively clean, the strength was improved from 180 MPa to 350 MPa. This improvement is consistent with the Hall–Petch equation which relates strength inversely to the square of the grain size [17]. Further improvements in processing could lead to smaller grains and potentially higher strengths. We also expect improvements in the surface polishing process to enhance strength.

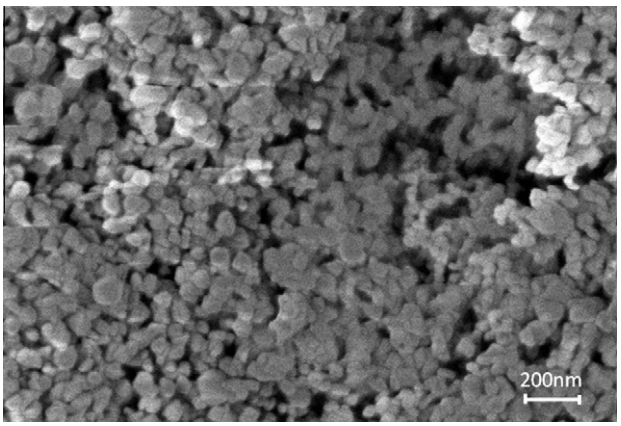

Fig. 1. SEM picture of spinel powder synthesized at NRL.

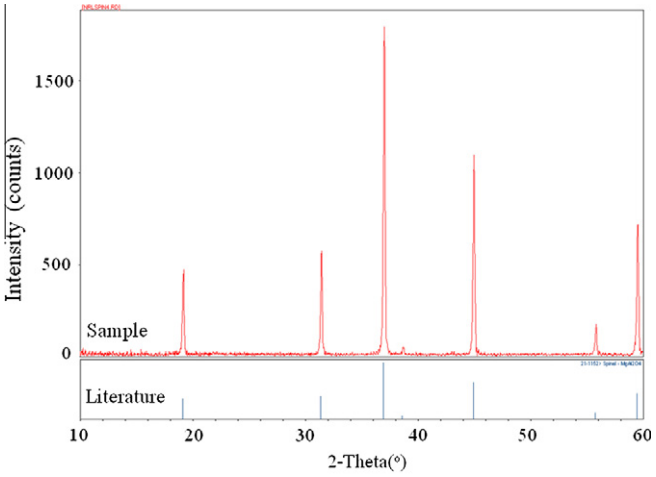

Fig. 2. X-ray diffraction pattern for synthesized spinel powder.

Table 1
Chemical analysis of commercial spinel powder and powder synthesized at NRL.

	Commercial powder (ppm)	NRL powder (ppm)
F	1000	<5
Na	500	3.5
Si	475	10
P	125	1.1
Cr	175	2.7
Fe	715	3.5
Ni	90	<0.5
Y	140	25
Zr	1400	1.5
Ce	365	0.70

Table 2 compares the physical properties of spinel with fused silica and OFG glass. All the properties of spinel were measured at University of Dayton Research Institute except for the absorption coefficient which was measured at the Naval Air Warfare Center (NAWC). Physical properties of OFG glass were obtained from the website of Infrared Fiber Systems [18] and Billman et al. [19]. Properties of fused silica were obtained from the literature [20] and Browder et al. [21]. In comparison with fused silica, spinel has comparable absorption coefficient, is about >2.5× harder, 7× stronger and has about 10× higher thermal conductivity. In comparison with the OFG glass, spinel has about 10× lower absorption coefficient, is >3.5× stronger and harder and has about 20× higher thermal conductivity. For airborne applications, the resistance to thermal shock becomes very important. Consequently, we have calculated the figure of merit for thermal shock (FOM-TS) [22]:

$$\text{FOM-TS} = S \cdot k(1-\upsilon)/\alpha \cdot E \quad (1)$$

where S is the strength, k is the thermal conductivity, υ is the Poisson's ratio, α is the thermal expansion coefficient and E is the Young's modulus. We have calculated values for the FOM-TS using

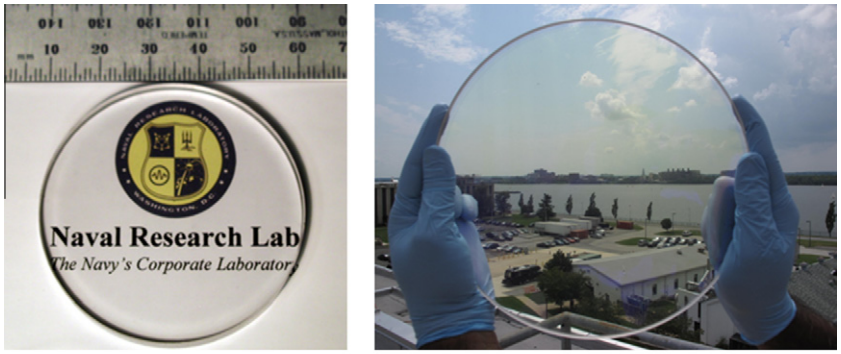

Fig. 3. (a) An uncoated 5 cm diameter spinel window and (b) a 10 in. diameter spinel window coated with broadband AR coatings, respectively.

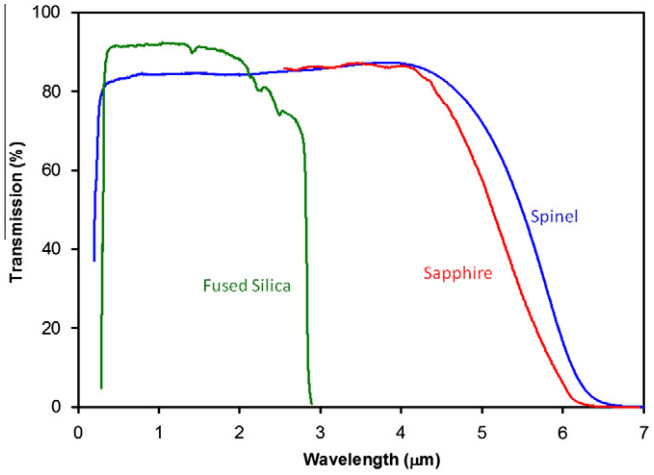

Fig. 4. Transmission spectrum of silica glass, sapphire and spinel ceramic.

values for the appropriate properties shown in Table 2. While silica has a high resistance to thermal shock attributed to its very low thermal expansion coefficient, the OFG glass has poor resistance to thermal shock, mainly attributed to its high thermal expansion coefficient. Spinel has higher resistance to thermal shock than silica glass, and more than 40 times higher than OFG glass. OFG glass, being an oxyfluoride, also has potentially inferior chemical and environmental durability compared with silica glass and spinel [23].

Rain and sand erosion tests performed on spinel ceramic were 100% successful. The spinel samples were able to withstand impact from rain droplets at speeds up to 600 mph and sand particles at speeds up to 460 mph without damage, without surface pitting and no change in transmission, unlike glass which exhibits considerable damage.

Initial spinel samples made using commercial powders had very high absorption losses due to impurities. Consequently, we developed an aqueous synthetic route for making higher purity spinel powders. This has resulted in a record low absorption loss of 6 ppm/cm at 1.064 μm (Fig. 5).

The performance of a window material in an HEL environment can be predicted using a figure of merit (FOM) [24]. The FOM for optical path distortion (OPD), expressed as FOM(OPD), is a combination of figure of merits for thermal distortion FOM(χ), temperature rise FOM(ΔT) and thickness FOM(L). Window materials with low FOM(OPD) are desired for better HEL performance:

$$\mathrm{FOM(OPD)} = \mathrm{FOM}(\chi)\cdot\mathrm{FOM}(\Delta T)\cdot\mathrm{FOM}(L) \quad (2)$$

The three FOM's are expressed as:

$$\mathrm{FOM}(\chi) = (n-1)\cdot(1+\nu)\cdot\mathrm{CTE} + dn/dT + n^3\cdot Y\cdot\mathrm{CTE}\cdot(q_{11}+q_{12})/4 \quad (3)$$

$$\mathrm{FOM}(\Delta T) = \alpha(\rho\cdot C_p) \quad (4)$$

$$\mathrm{FOM}(L) = \sqrt{((3+\nu)/\sigma_{\max})} \quad (5)$$

where n is refractive index, ν is Poisson's ratio, CTE is coefficient of linear thermal expansion, dn/dT is thermo-optic coefficient (change in refractive index as a function of temperature), Y is Young's modulus, q_{11}, q_{12} are stress optic coefficients in directions parallel and perpendicular to the load, respectively, α is absorption coefficient, ρ is density, C_p is heat capacity at constant pressure, and $\sigma_{\max}$ is

Table 2
Comparison of the optical, mechanical and thermal properties of spinel with fused silica and OFG glass.

Property measurements	Fused silica	OFG glass	SPINEL
Optical			
Absorption coefficient (ppm cm^{-1} at 1.06 μm)	10	75	6
Refractive Index (at 1.06 μm)	1.45	1.45	1.707
dn/dt (K^{-1} at 1.3 μm)	12×10^{-6}	-9.2×10^{-6}	23×10^{-6}*
Stress optic coefficient (Pa^{-1})	3.4×10^{-13}	4.1×10^{-13}	3×10^{-13}
Mechanical			
Density (g/cm^3)	2.2	3.75	3.58
Poisson's ratio	0.17	0.31	0.26
Hardness (kg/mm^2)	600	500 (est)	1645
Fracture strength (MPa)	50	102	350
Young's modulus (GPa)	74.5	69.6	282
Thermal			
Thermal expansion coeff. (K^{-1})	0.5×10^{-6}	14.9×10^{-6}	5.9×10^{-6}
Thermal capacity C_p (J/g/K)	0.74	0.67	0.604
Thermal conductivity (W/m K)	1.38	0.7	13.407
Figure of merit for thermal shock (FOM-TS)	1537	47	2086

* at 633 nm.

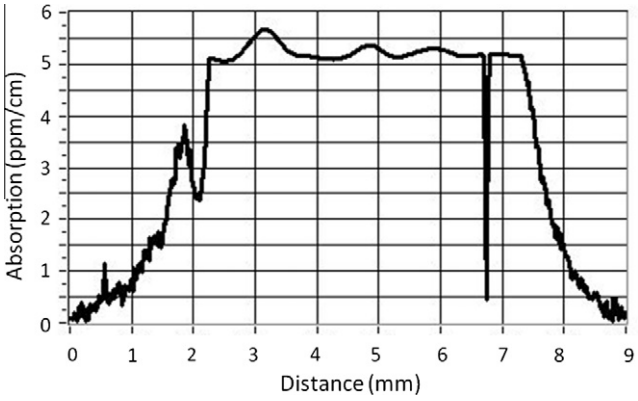

Fig. 5. Absorption coefficient of spinel at a wavelength of 1.06 μm.

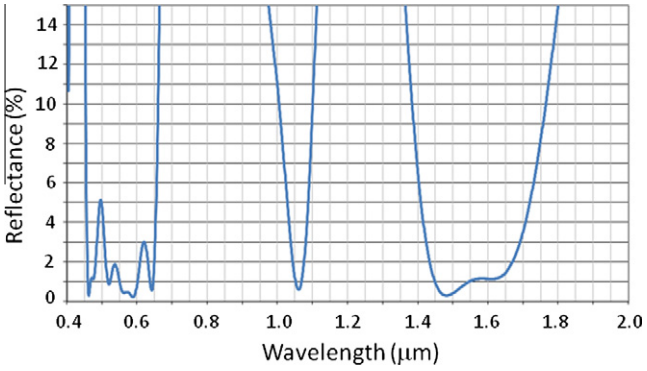

Fig. 7. The measured reflection loss for a 5 cm diameter spinel ceramic with broadband AR coatings designed for the visible, 1.06 μm and 1.45–1.65 μm.

fracture strength. The FOM(OPD) was calculated using the physical properties from Table 2 and is plotted in Fig. 6. The FOM(OPD) of spinel is about half of that for commercial grade fused silica and comparable to ultra-high purity silica. Since it has significantly better environmental ruggedness, this makes spinel an excellent candidate for a high energy laser window, especially those operating in hostile environments. The FOM(OPD) of spinel can be further improved by increasing its strength. A stronger window will impact the thickness FOM(L), thereby reducing the window thickness. Higher strengths will also manifest into lighter windows, key in airborne applications.

The FOM(OPD) of OFG glass is low because of its negative dn/dT, but it has very poor thermal conductivity and a large CTE. This manifest into a 40× lower thermal shock resistance than spinel, and so poses potential problems for airborne applications.

Hard, abrasion resistant and low absorption loss anti-reflection coatings are needed for HEL applications to reduce the Fresnel reflection losses which are about 6.5% per face. The broadband coatings were designed for the visible, 1.06 μm and 1.45–1.65 μm and were applied to both surfaces on 5 cm diameter spinel samples. The reflectance spectrum is shown in Fig. 7. Coatings were also applied which reduced the reflection loss from 6.5% to <0.1% per surface at 1.06 μm. Metrology was performed on the AR coated spinel substrates to fully characterize the coatings. The results, as summarized in Table 3, demonstrate that the AR coatings are rugged and have a relatively low absorption loss of 65 ppm. These coatings were also deposited on a large 10 in. diameter spinel window made from commercial powder (shown in Fig. 3).

Table 3
Metrology performed on the AR coated spinel ceramic.

Property	Method	Results
Adhesion	Mil-C-675C	Pass
Abrasion	Mil-C-48497	Pass
Surface roughness	Atomic force microscopy (AFM)	<2 nm
Absorption coefficient	Photo-thermal common path interferometry (PTCPI)	65 ppm/cm at 1064 nm

3.2. Yb^{3+} doped Y_2O_3 ceramic

Precipitation followed by calcination at 600 °C produced a powder with submicron particle size (Fig. 8) and about two orders of magnitude lower impurity content (Table 4). The structural phase was confirmed using X-ray diffraction analysis. A slight shift in the

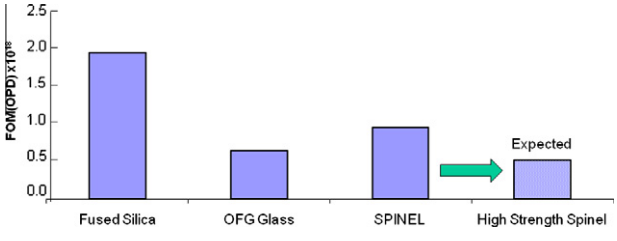

Fig. 6. The figure of merit for optical path distortion, FOM(OPD) comparing spinel ceramic with silica and OFG glass. The expected FOM(OPD) for spinel is based on a higher strength ceramic obtained using a smaller grain size.

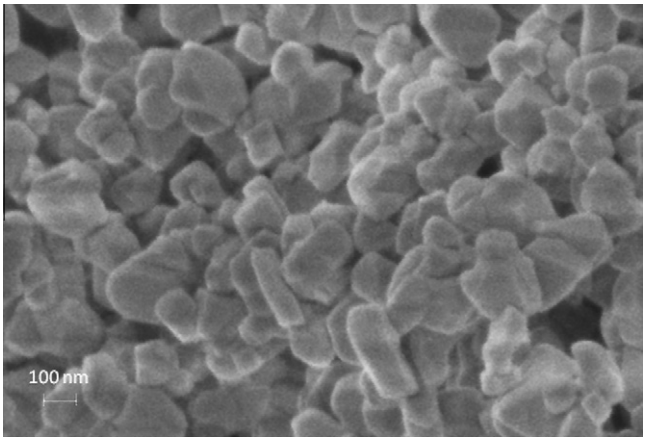

Fig. 8. SEM image of submicron 10% Yb^{3+} doped Y_2O_3 powder made by precipitation followed by calcination at 600 °C.

Table 4
Chemical analysis of commercial Yb:Y_2O_3 powder and powder synthesized at NRL.

Element	Commercial (ppm)	NRL (ppm)
B	500	0.75
Si	185	19
P	60	6.0
S	1600	5.5
Cl	10,000	10
Fe	610	6.5
Zn	5.2	<0.2
La	50	1.2
Ce	30	0.2
Nd	29	0.15
Eu	322	1.0
Gd	1700	0.25
Tb	10	0.11
Er	1.5	0.56

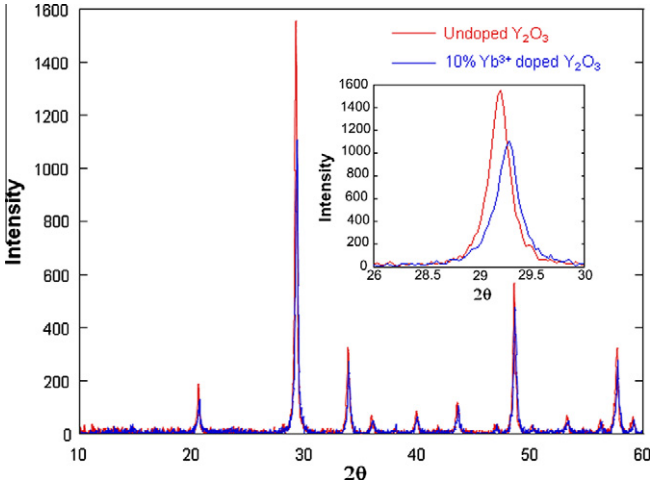

Fig. 9. The X-ray diffraction pattern for undoped Y_2O_3 powder and 10% Yb^{3+} doped Y_2O_3 powder. The expected small shift in the peak positions is highlighted in the insert.

Fig. 10. A picture of a 1 in. diameter 2% Yb^{3+} doped Y_2O_3 transparent ceramic.

lattice parameters was observed on doping Yb^{3+} in Y_2O_3 attributed to the small difference in the cation size. The shift was more pronounced for a 10% Yb^{3+} doped Y_2O_3 powder (Fig. 9).

The density of a 2% Yb doped ceramic sample was 5.11 g/cm^3, which is in excellent agreement with 5.11 g/cm^3 based on first principle calculations using a density of weighted mixtures of Y_2O_3 (5.03 g/cm^3) and Yb_2O_3 (9.17 g/cm^3). The refractive index increases with Yb^{3+} addition, presumably due to the higher polarizability of the Yb^{3+} ion compared with the Y^{3+} ion. For example,

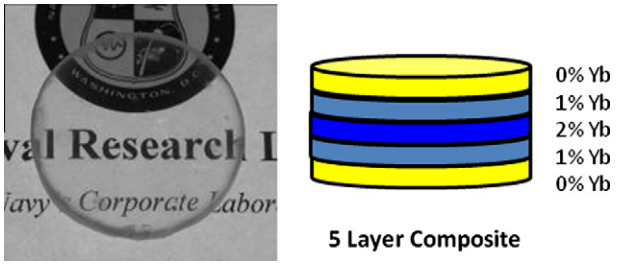

Fig. 11. Picture and schematic of a ceramic composite.

the refractive indices of Y_2O_3 and 2% Yb doped Y_2O_3 are 1.8831 and 1.8857, respectively, at a wavelength of 1 μm. The fluorescence lifetime of the 2% Yb^{3+} doped ceramic was 1 m s and same as the powder used to make the ceramic. This bodes well for making a laser since it implies that the ceramization process did not adversely impact the rare earth ion sites. Fig. 10 shows a picture of the transparent ceramic. Additionally, 1 in. diameter composite ceramic samples containing five-layers were prepared as shown in Fig. 11, where the thickness of each layer was approximately 1 mm. The ability to use undoped ceramic endcaps enables control of thermal loads on the endface. Furthermore, grading of the rare earth ion dopant profile will result in more uniform absorption along the length providing uniform gain and better thermal control in the gain medium. The spatial profile of Yb^{3+} was obtained by detection of the green upconversion fluorescence on pumping at 940 nm. Results demonstrated that inter-diffusion of Yb^{3+} ions was less than 100 μm at the temperatures used to make the ceramics.

Fig. 12 shows the absorption and emission spectra for the 2% Yb doped Y_2O_3 ceramics. The spectra highlight the convenience of diode pumping at about 940 and 980 nm, and potential for lasing at around 1030 and 1080 nm, respectively.

Fig. 13 shows the laser output power at 1076 nm obtained using CW pumping at 940 nm on uniformly doped 2% Yb^{3+}:Y_2O_3 ceramic samples which were about 2 mm thick and 3 mm in diameter. Up to 600 mW output power was demonstrated with a slope efficiency of 36.7% using a 2% output coupler. A slope efficiency of 44.6% was demonstrated using a 5% output coupler. In order to estimate losses within the ceramic, the method of Findlay and Clay [25] was applied. The calculated roundtrip loss for this sample was approximately 4%. The preliminary results for a five layer composite ceramic are also shown in Fig. 14. The slope efficiencies were 4.1%, 5.8% and 7.5% using output couplers of 1%, 2% and 5%, respectively. These efficiencies can be increased with improved processing. The calculated round trip loss for this sample, like that of the single component sample, was approximately 4%. In addition,

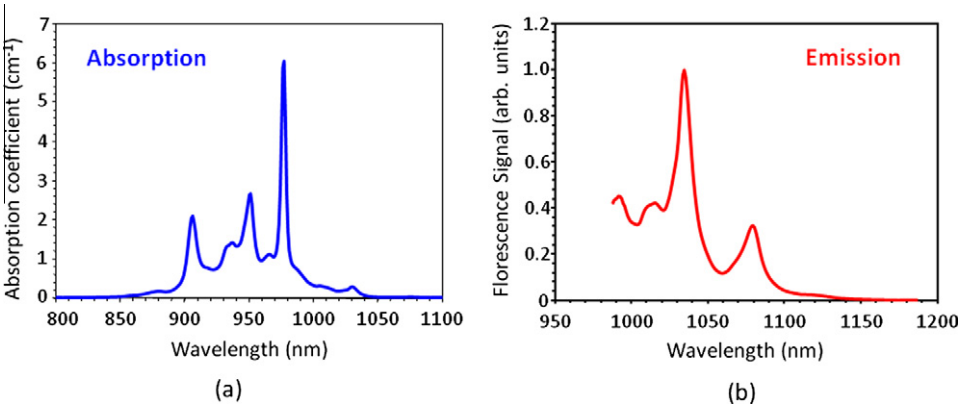

Fig. 12. (a) The absorption and (b) emission spectra for the 2% Yb^{3+} doped Y_2O_3 ceramics.

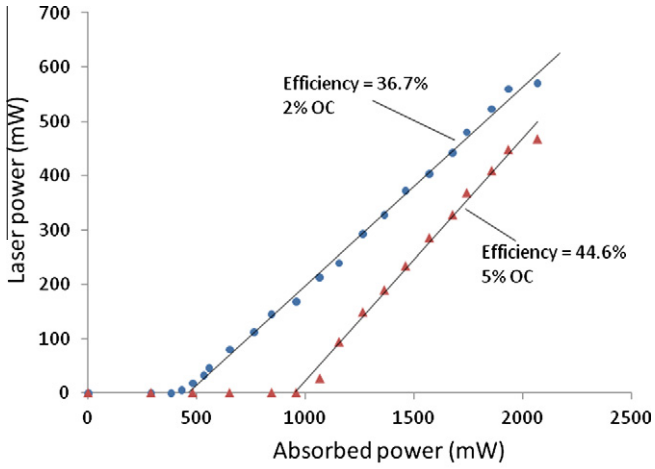

Fig. 13. The laser output power at 1076 nm obtained using CW pumping at 940 nm on uniformly doped 2% Yb^{3+}:Y_2O_3 ceramic samples which were about 2 mm thick and 3 mm in diameter.

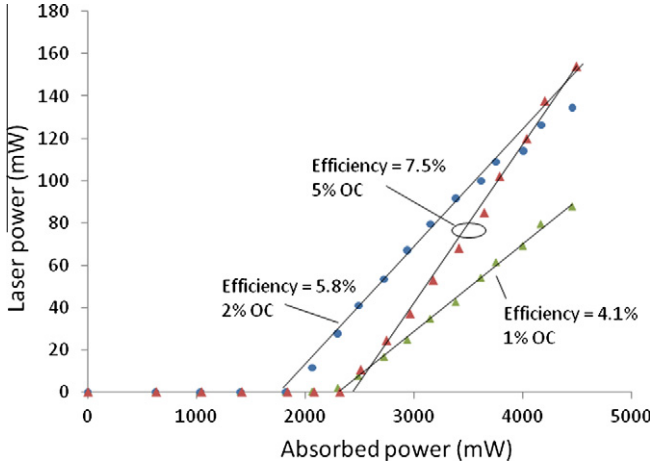

Fig. 14. The preliminary lasing results for a five layer composite ceramic shown in Fig. 11.

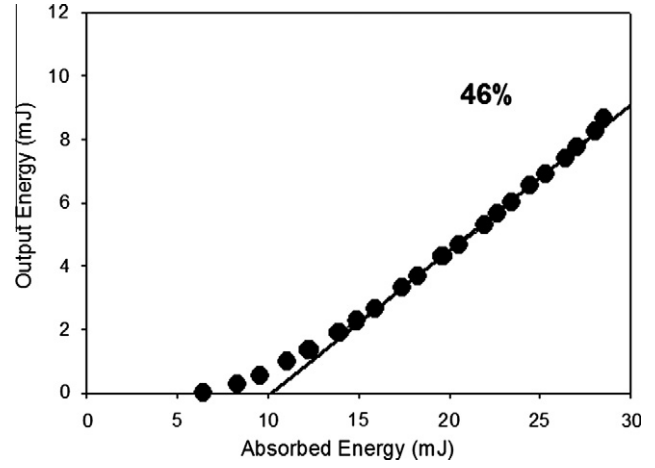

Fig. 15. Pulsed lasing results for the 2% Yb^{3+}:Y_2O_3 doped ceramic samples. Lasing occurred at 1077 nm with a slope efficiency of 46%.

pulsed lasing experiments were performed on similar 2% Yb^{3+}:Y_2O_3 doped ceramic samples. Lasing occurred at 1077 nm with a slope efficiency of 46% (Fig. 15). Both the CW and pulsed lasing results represent the first demonstration of lasing using hot pressed Yb^{3+}:Y_2O_3 ceramic materials.

4. Conclusions

Spinel is a rugged ceramic material which transmits from the UV to 5 μm and could be used as an exit aperture for HEL systems. However, spinel made from commercial powder exhibits high absorption losses due to extrinsic impurities. So we have developed an aqueous process to make high purity spinel powders. Ceramic samples made from these powders demonstrated a record low absorption loss of 6 ppm/cm at 1.06 μm. We also developed and demonstrated rugged and low absorption loss AR coatings. The spinel ceramic was fully characterized and identified as an excellent candidate for HEL window applications, especially in hostile environments. It is more than three times stronger and harder than glass, with >10× higher thermal conductivity and with up to 40× higher thermal shock resistance.

To date, laser quality Yb:Y_2O_3 ceramic has only been previously made using vacuum sintering. However, we report, for the first time, lasing in hot pressed Yb^{3+}:Y_2O_3 ceramic made from co-precipitated powder. The ceramic lased in both cw and pulsed mode with approximately 45% slope efficiency. Additionally, we demonstrated preliminary lasing in a five-layered composite containing undoped endcaps. Future work is aimed at lowering the scattering losses which will increase the laser slope efficiency to >80%. This work also paves the way forward for engineering geometries for better thermal management compared with their single crystal counterparts in materials with higher thermal conductivity than YAG.

Acknowledgements

This program was funded by the High Energy Laser Joint Technology Office (HEL-JTO) and the Office of Naval Research. The authors would like to acknowledge the collaboration with MER Corp. (Tucson, AZ) for demonstrating scale-up to a 12 in. × 16 in. ceramic spinel window.

References

[1] C.A. Klein, Figures of merit for high-energy laser-window materials: thermal lensing and thermal stresses, SPIE 6403 (2007) 640308-1–640308-16.
[2] S. Bayya, J.S. Sanghera, I.D. Aggarwal, G. Chin, Vis-IR transmitting window materials, SPIE 5786 (2005) 262–271.
[3] A. Heller, Sci. Technol. Rev., April 2006, p. 10.
[4] B. Bishop, Northrop Grumman scales new heights in electric laser power, achieves 100 kW from a solid-state laser, Globe Newswire, March 18, 2009.
[5] Textron Achieves Over 100 kW with Laser, Photonics.com, February 22, 2010.
[6] K. Ueda, J.-F. Bisson, H. Yagi, K. Takaichi, A. Shirakawa, T. Yanagitani, A.A. Kaminskii, Scalable ceramic lasers, Laser Phys. 15 (2005) 927–938.
[7] A. Ikesue, Y.L. Aung, Synthesis and performance of advanced ceramic lasers, J. Am. Ceram. Soc. 89 (6) (2006) 1936–1944.
[8] A. Brenier, G. Boulon, Overview of the best Yb^{3+}-doped laser crystals, J. Alloys Compd. 323–324 (2001) 210–213.
[9] David W. Reicher, Roberto Christian, Patrick Davidson, Stanley Z. Peplinski, Use of multiple DC magnetron deposition sources for uniform coatings of large areas, Proc. SPIE 7409 (2009) 740909.
[10] Alexei Alexandrovski, Martin Fejer, Ashot Markosyan, Roger Route, Photothermal common-path interferometry (PCU): new developments, Proc. SPIE 7193 (2009) 71930D.
[11] R.J. Harris, G.T. Johnston, G.A. Kepple, P.C. Krok, H. Mukai, Infrared thermooptic coefficient measurement of polycrystalline ZnSe, ZnS, CdTe, CaF_2, and BaF_2, single crystal KCl and Tl-20 glass, Appl. Opt. 16 (1977) 436–438.
[12] Shyam S. Bayya, Geoffrey D. Chin, Jasbinder S. Sanghera, Ishwar D. Aggarwal, John A. Detrio, Thermo-optic coefficient of barium gallogermanate glass, Appl. Opt. 46 (32) (2007) 7889–7891.
[13] ASTM method C770, Standard Test Method for Measurement of Glass Stress – Optical Coefficient.

[14] ASTM method C 1259, Standard Test Method for Dynamic Young's Modulus, Shear Modulus, and Poisson's Ratio for Advanced Ceramics by Impulse Excitation of Vibration.
[15] ASTM E1269, Standard Test Method for Determining Specific Heat Capacity by Differential Scanning Calorimetry.
[16] ASTM E1461-07, Standard Test Method for Thermal Diffusivity by the Flash Method.
[17] C.S. Pande, K.P. Cooper, Nanomechanics of Hall–Petch relationship in nanocrystalline materials, Prog. Mater. Sci. 54 (2009) 689–706.
[18] <http://www.infraredfibersystems.com/ioptics_specs.htm>.
[19] Kenneth W. Billman, Danh C. Tran, Ken H. Levin, Steven M. Daigneault, Nathan J. Edwards, Progress toward an athermal HEL optical window, Proc. SPIE 5647 (2005) 207–223.
[20] <http://www.sciner.com/Opticsland/FS.htm>.
[21] J.S. Browder, S.S. Ballard, P. Klocek, Physical properties of crystalline infrared materials, in: P. Klocek (Ed.), Handbook of Infrared Materials, Mercel Dekker Inc. Publications, 1991, pp. 193–425.
[22] Daniel C. Harris, Materials for Infrared Windows and Domes: Properties and Performance, SPIE Press, 1999.
[23] C.T. Moynihan, S.R. Loehr, Chemical durability of fluoride glasses, Mater. Sci. Forum 32–33 (1998) 243–254.
[24] S.S. Bayya, G.D. Chin, J.S. Sanghera, I.D. Aggarwal, Germanate glass as a window for high energy laser systems, Opt. Exp. 14 (24) (2006) 11687–11693.
[25] D. Findlay, R.A. Clay, The measurement of internal losses in 4-level lasers, Phys. Lett. 20 (1966) 277–278.

Please cite this article in press as: J. Sanghera et al., Opt. Mater. (2010), doi:10.1016/j.optmat.2010.10.038